Electrospun graphene decorated MnCo$_2$O$_4$ composite nanofibers for glucose biosensing

Yuting Zhang [a], Shuai Liu [a], Yu Li [a], Dongmei Deng [b,*], Xiaojing Si [a], Yaping Ding [a], Haibo He [a], Liqiang Luo [a,*], Zhenxin Wang [c,*]

[a] Department of Chemistry, College of Sciences, Shanghai University, Shanghai 200444, PR China
[b] Department of Physics, College of Sciences, Shanghai University, Shanghai 200444, PR China
[c] State Key Laboratory of Electroanalytical Chemistry, Changchun Institute of Applied Chemistry, Chinese Academy of Sciences, Changchun 130022, PR China

ARTICLE INFO

ABSTRACT

Graphene decorated MnCo$_2$O$_4$ composite nanofibers (GMCFs) were synthesized by electrospinning and subsequent calcination in an Ar atmosphere. The structural and morphological characterizations of GMCFs were performed using X-ray diffraction, Fourier transform infrared spectroscopy, Raman spectroscopy, energy-dispersive spectroscopy, scanning electron microscopy and transmission electron microscopy. The synthesized GMCFs combine the catalytic activity of spinel-type MnCo$_2$O$_4$ with the remarkable conductivity of graphene. In addition, electrospinning can process MnCo$_2$O$_4$ materials into nanosized architectures with large surface area to prevent magnetic nanoparticles from aggregating. The obtained GMCFs were applied as a novel platform for glucose biosensing. Electrochemical studies show that the developed biosensor exhibits excellent electrocatalytic activity towards glucose oxidation over a wide linear range of 0.005–800 μM with a low detection limit of 0.001 μM.

1. Introduction

Graphene, a two-dimensional monolayer of sp^2-bonded carbon atoms with a honeycomb structure, has captured considerable attention due to its huge surface area, excellent electrical conductivity, good biocompatibility, unique mechanical and thermal properties (Novoselov et al., 2004; Geim and Novoselov, 2007; Hummers and Offeman, 1958; Niyogi et al., 2006; Wang et al., 2012; Meyer et al., 2007). Thanks to these outstanding advantages, graphene has been applied in numerous areas including optical devices, energy storage, supercapacitors and sensors (Liu et al., 2011; Yang et al., 2013; Zhang et al., 2013; Shan et al., 2009). However, graphene tends to lose large specific surface area and outstanding electric property owing to unavoidable aggregation caused by Van der Waals forces and strong π–π stacking (Lv et al., 2009; Stoller et al., 2008.; Wu et al., 2013). To prevent graphene from aggregating, the development of desirable strategies to synthesize well-dispersed graphene-based nanocomposite remains a great challenge.

Nowadays, electrospinning technology has proved to be an effective and convenient method for synthesizing exceptionally long fibers with diameters ranging from several micrometers to tens of nanometers (B. Ding et al., 2010; Li and Xia, 2004; Saquing et al., 2009). In a typical electrospinning process, a high voltage is applied to a polymer solution, deforming the pendent drop at the tip of the spinnerette into a conical shape referred to as the "Taylor cone", and then the polymer solution is ejected from the tip to a collector (Lin et al., 2009; Tang et al., 2010). The remarkable specific surface area, high porosity and good structural controllability of electrospun nanomaterials make them successfully applied in many fields, such as sensors, separation technology, batteries and supercapacitors (Ouyang et al., 2013; Yoshimatsu et al., 2008; Nan et al., 2013; Dong et al., 2013).

The spinel-type oxides with the formula AB$_2$O$_4$ have attracted a great deal of research interest linked to a wide range of applications including magnetism, electronics, energy storage and catalysis owing to their fascinating magnetic, electrical, optical and catalytic properties (F.Y. Cheng et al., 2011; Hu et al., 2012; Liang et al., 2012). Spinel-type oxide materials exhibit synergistic enhancement in electrocatalytic activity that is much better than a simple combination of individual metal oxide (Jo et al., 2012; Paudel et al., 2011). This is essentially related to: (i) The unit cell of spinel contains eight face centered cubic formed by oxygens, where only one-eighth of the 64 tetrahedral sites are occupied by A ions and one-half of the 32 octahedral sites by B ions; (ii) The great flexibility of the structure in hosting various metal ions, with a large possibility of reciprocal substitution between them (Li et al., 2004; Zeng et al., 2008.; Huang et al., 2011).

* Corresponding authors.
E-mail addresses: dmdeng@shu.edu.cn (D. Deng), luck@shu.edu.cn (L. Luo), wangzx@ciac.jl.cn (Z. Wang).

Reliable and fast determination of glucose is of immense scientific and technological importance in many areas such as biotechnology, clinical diagnostics and food industry (Wu et al., 2010; Heller and Feldman, 2008; Li and Lin, 2007; Newman and Turner, 2005). As the most common class of electrochemical biosensors, glucose oxidase (GOx) modified electrodes have been extensively studied over the last four decades because of the high demand of sensitive and reliable blood glucose monitoring in biological and clinical aspects (Zou et al., 2008; Wang et al., 2003). However, the GOx-based biosensors have some disadvantages, such as instability, high cost of enzymes and complicated immobilization procedure (Wang et al., 2008; Wilson and Turner, 1992). Therefore, the development of highly selective, sensitive, reliable electrocatalysts as alternative to GOx is still imperatively needed.

In our previous work, spinel-type $MnCo_2O_4$ nanofibers (MCFs) have been successfully synthesized by electrospinning and employed as electrocatalysts for the oxidation of glucose (Zhang et al., 2014). However, it is still a great task to develop composite materials with better activity, conductivity and sensitivity for bioelectrocatalysis. Graphene could be chosen as a conductive additive to enhance the electrocatalytic performance of electrospun MCFs. In this study, we considered unifying the conductivity of graphene and the electrocatalytic activity of spinel-type $MnCo_2O_4$ nanofibers. Graphene as a conductive additive enhance the electron transfer rate of spinel nanofibers, while electrospun spinel nanofibers as supports are of great benefit to the distribution of graphene. To the best of our knowledge, no published report dealing with this synthesis of graphene decorated $MnCo_2O_4$ composite nanofibers (GMCFs) by electrospinning is available until now according to the literature survey. Extensive characterizations of GMCFs were studied using X-ray diffraction (XRD), Fourier transform infrared (FT-IR) spectroscopy, Raman spectroscopy, energy-dispersive spectroscopy (EDS), scanning electron microscopy (SEM) and transmission electron microscopy (TEM). The synthesized GMCFs were employed as electrocatalysts for the oxidation of glucose.

2. Experimental

2.1. Regents and apparatus

Graphite oxide (GO) was obtained from Nanjing XFNANO Materials Tech Co., Ltd, (China). Hydrazine hydrate ($NH_2NH_2 \cdot H_2O$, 80%), polyvinyl pyrrolidone (PVP, $M_W = 1,300,000$) and $Mn(Ac)_2 \cdot 4H_2O$ were obtained from Aladdin Chemical Reagent Co., Ltd. (China). $Co(Ac)_2 \cdot 4H_2O$, N,N-dimethylformamide (DMF), $Mn(NO_3)_2 \cdot 6H_2O$, $Co(NO_3)_2 \cdot 6H_2O$, $K_3Fe(CN)_6$, $K_4Fe(CN)_6 \cdot 3H_2O$, potassium chloride (KCl) and sodium hydroxide (NaOH) were

purchased from Sinopharm Chemical Reagent Co., Ltd. (China). Glucose was provided by Sigma (USA). All other chemicals were of analytical grade and Milli-Q water (18.25 MΩ cm) was used throughout the experiments.

XRD pattern was obtained on Rigaku DLMAX-2200 X-ray diffraction using K radiation ($\lambda = 1.5418$ Å, 40 kV, 40 mA; scanning rate: $0.08° \text{ s}^{-1}$) in the range of 10–80°. FT-IR spectra were recorded in 400–4000 cm^{-1} region on AVATAR 370 Fourier transform infrared spectrometer (America). Raman spectra were carried out with Renishaw in via-Reflex using 633 nm at room temperature (INVIA, England). SEM images were performed on scanning electron microscope (JSM-6700F, Japan) at 15 kV, equipped with EDS analyzer. TEM images were recorded with transmission electron microscope (JEM-2010F, Japan) at 200 kV. The electrochemical experiments were carried out on CHI 660D electrochemical workstation (Shanghai CH Instrument Co., China) with a conventional three-electrode system, in which the modified glassy carbon electrode (GCE), saturated calomel electrode (SCE) and a platinum foil served as working, reference and counter electrodes, respectively.

2.2. Preparation of GMCFs nanofibers

Graphene was prepared according to the published route involving the steps of graphite oxidation, exfoliation and chemical reduction (Zhu et al., 2012; Kovtyukhova et al., 1999). Briefly, 5 mg GO was dispersed in 50 mL water, and the dispersion was exfoliated by sonicating at room temperature for 40 min. Then, $NH_2NH_2 \cdot H_2O$ (1% v/v) was added into the GO dispersion. The resulting mixture was heated to 100 °C and kept stirring for 24 h. Subsequently, the solution was filtered, and the filtrate was discarded. Finally, black hydrophobic powder graphene was obtained by drying in vacuum at 60 °C, and stored at ambient conditions.

Scheme 1 illustrates the major steps involved in the synthesis of GMCFs. First, to prepare the electrospinning solution, 0.0033 g freshly prepared graphene in 10 mL DMF was sonicated for 12 h to disperse graphene. Then, 1.6747 g PVP was added to the above solution, followed by ultrasonic stir for 12 h. After that, 0.3515 g $Mn(Ac)_2 \cdot 4H_2O$ and 0.7030 g $Co(Ac)_2 \cdot 4H_2O$ were slowly added into the above mixture and stirred continuously for another 12 h to yield russet homogeneous solution. The mixture was immediately loaded into a plastic syringe equipped with a stainless steel needle. The electrospinning process was performed in an electric field of 180 kV m^{-1} by applying a high voltage of 18 kV, with 10 cm spacing between the needle tip and the collector (aluminum foil). The feeding rate for the precursor solution was 1 mL h^{-1} using a syringe pump. The electrospinning process was conducted in air with 50% relative humidity. After electrospinning, the graphene/$Mn(Ac)_2$/$Co(Ac)_2$/PVP composite fibers were dried in a drying oven at 75 °C for 12 h. Finally, the dried fibers were

acetate

PVP

DMF

graphene/acetate/PVP solution

syringe

collect

graphene/acetate/PVP composite fibers
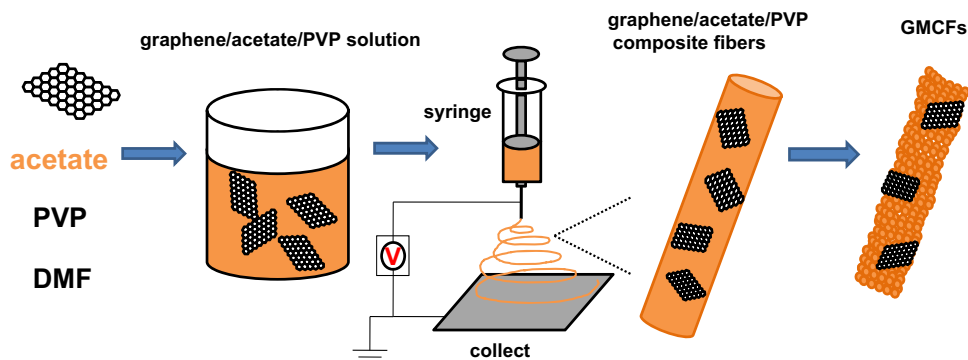
GMCFs

Scheme 1. The major steps involved in the synthesis of GMCFs.

calcined at 650 °C for 2 h in a protective atmosphere of Ar with 2.5 °C min^{-1} from room temperature to 650 °C. For comparison, spinel $MnCo_2O_4$ samples were prepared by electrospining (named as MCFs) and hydrothermal method (named as MCNPs) (see Supporting information).

2.3. Fabrication of GMCF/GCE

Prior to surface modification, the GCE was polished carefully with 1.0, 0.3 and 0.05 μm alumina powder, respectively. The polished GCE was then rinsed successively with nitric acid (1:1), absolute alcohol and water, respectively. After that, a certain amount of GMCFs were dispersed in 1 mL water by ultrasonic agitation to obtain a homogenous suspension. Finally, 10 μL of the suspension was cast on the surface of GCE and GMCF/GCE was allowed to dry under an infrared lamp. At the same time, MCF/GCE was also prepared by similar procedure to compare with GMCF/GCE.

3. Results and discussion

3.1. XRD, FT-IR and Raman spectroscopy characterization

The crystal structure of GMCFs was characterized by XRD and the diffraction peaks are clearly observed in Fig. 1A. The characteristic reflections at $2\theta = 18.55°$, 30.54°, 36.00°, 43.76°, 54.34°, 57.91°, 63.62° and 75.30° corresponded to the (111), (220), (311), (400), (422), (511), (440) and (533) phase structure of $MnCo_2O_4$, respectively. All the detectable diffraction peaks can be indexed as face-centered cubic spinel phase $MnCo_2O_4$ with space group Fd3m (JCPDS card no. 23-1237), indicating that the presence of graphene within MCFs does not affect the formation of spinel cubic phase (Zhu and Gao, 2009).

FT-IR spectra were employed to prove the removal of polymer and the formation of spinel structure in GMCFs. Fig. 1B shows the FT-IR spectra of the graphene/Mn(Ac)$_2$/Co(Ac)$_2$/PVP composite fibers and those calcined at 650 °C. The peaks in the range of 1000–3600 cm^{-1} are the characteristic absorption peaks of graphene/Mn(Ac)$_2$/Co(Ac)$_2$/PVP composite fibers (Borodko et al., 2006; F.Y. Cheng et al., 2011; Y.L. Cheng et al., 2011). Specifically, the intensive broadband centered at 3415 cm^{-1} was assigned to O–H stretching vibration interacting through H bonds. The band at 2954 cm^{-1} was the C–H asymmetric stretching vibration mode due to the CH$_2$ groups of the long aliphatic alkyl groups. The stretching vibration of the carboxylate group was observed at 1654 cm^{-1} and the band at 1022 cm^{-1} corresponded to acetate ion traces. When the composite fibers were calcinated at 650 °C

(curve b), all the peaks belonging to PVP disappeared and two new peaks appeared at 544 and 632 cm^{-1}, representing the vibrational bending modes of $\nu_{Co–O}$ and $\nu_{Mn–O}$ in the tetragonal $MnCo_2O_4$ spinel (Rojas et al., 1994; Imran et al., 2013). These results indicate the decomposition of PVP and the crystallization of the spinel structure.

The presence of graphene phase in $MnCo_2O_4$ was confirmed using Raman spectroscopy. Fig. 1C shows the Raman spectra of MCFs and GMCFs recorded from 200 to 2000 cm^{-1}. In the Raman spectrum of MCFs (curve a), the bands at 680 and 450 cm^{-1} can be ascribed to the A$_{1g}$ and E$_g$ modes of spinel $MnCo_2O_4$, respectively (Rousseau et al., 1981; Hou et al., 2011; Chen et al., 2011). Meanwhile, in the Raman spectrum of GMCFs (curve b), the broad D-band (defect-induced mode) at 1310–1350 cm^{-1} and G band (E$_{2g2}$ graphite mode) at 1570–1600 cm^{-1} were observed (Ferrari et al., 2006; Lucchese et al., 2010), indicating successful incorporation of graphene into the MCFs matrix.

3.2. SEM, TEM and EDS characterization

Fig. 2A shows morphology of the as-prepared graphene. Graphene were crumpled and wrinkled transparent flake-like structure on the surface of glassy carbon substrate, which provided well-exfoliated structure for binding to the surface of nanofibers. To confirm the priority of the electrospinning method, we synthesized the MCNPs by hydrothermal method. As can be seen from SEM image of MCNPs (Fig. 2B), the particle sizes were 100–300 nm, and nanoparticles aggregated heavily, which might be caused by the magnetic dipolar attraction of magnetic nanoparticles. Fig. 2C and D shows SEM images of electrospun GMCFs before and after calcination at 650 °C. After calcination at 650 °C, the diameter of the nanofibers decreased from 300 ± 50 to 150 ± 50 nm and the surfaces of the nanofibers were no longer smooth, which should be attributed to the loss of PVP from the nanofibers and the crystallization of $MnCo_2O_4$ spinel. In Fig. 2D, each individual nanofiber consisted of numerous $MnCo_2O_4$ nanoparticles stacked along the nanofiber length, which may provide a larger accessible surface area for the electrocatalytic oxidation of glucose (as discussed below). In addition, the agglomeration phenomenon was effectively eliminated through the electrospinning process. The presence of graphene phase was not revealed by SEM, possibly due to its low phase contrast and concentration in the matrix. SEM images of MCFs before and after calcination at 650 °C are shown in Fig. 2E and F. MCFs exhibited morphologies similar to those of GMCFs, whereas GMCFs possessed longer branches morphology than MCFs, which may be due to the encapsulation and wind of graphene.
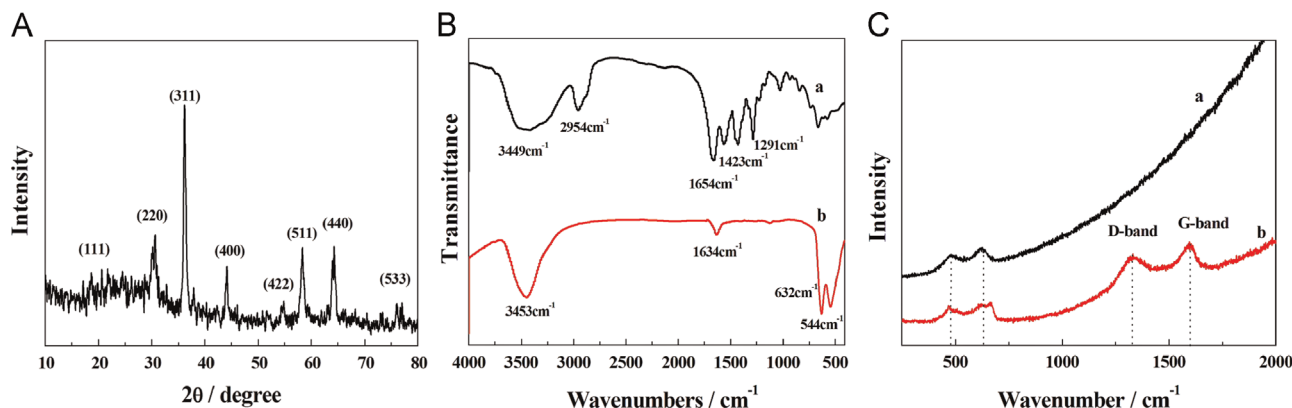

Fig. 1. (A) XRD pattern of electrospun GMCFs; (B) FT-IR spectra of fiber samples: (a) graphene/Mn(Ac)$_2$/Co(Ac)$_2$/PVP composite fibers, (b) composite fibers calcined at 650 °C; (C) Raman spectra of electrospun MCFs (curve a) and GMCFs (curve b).
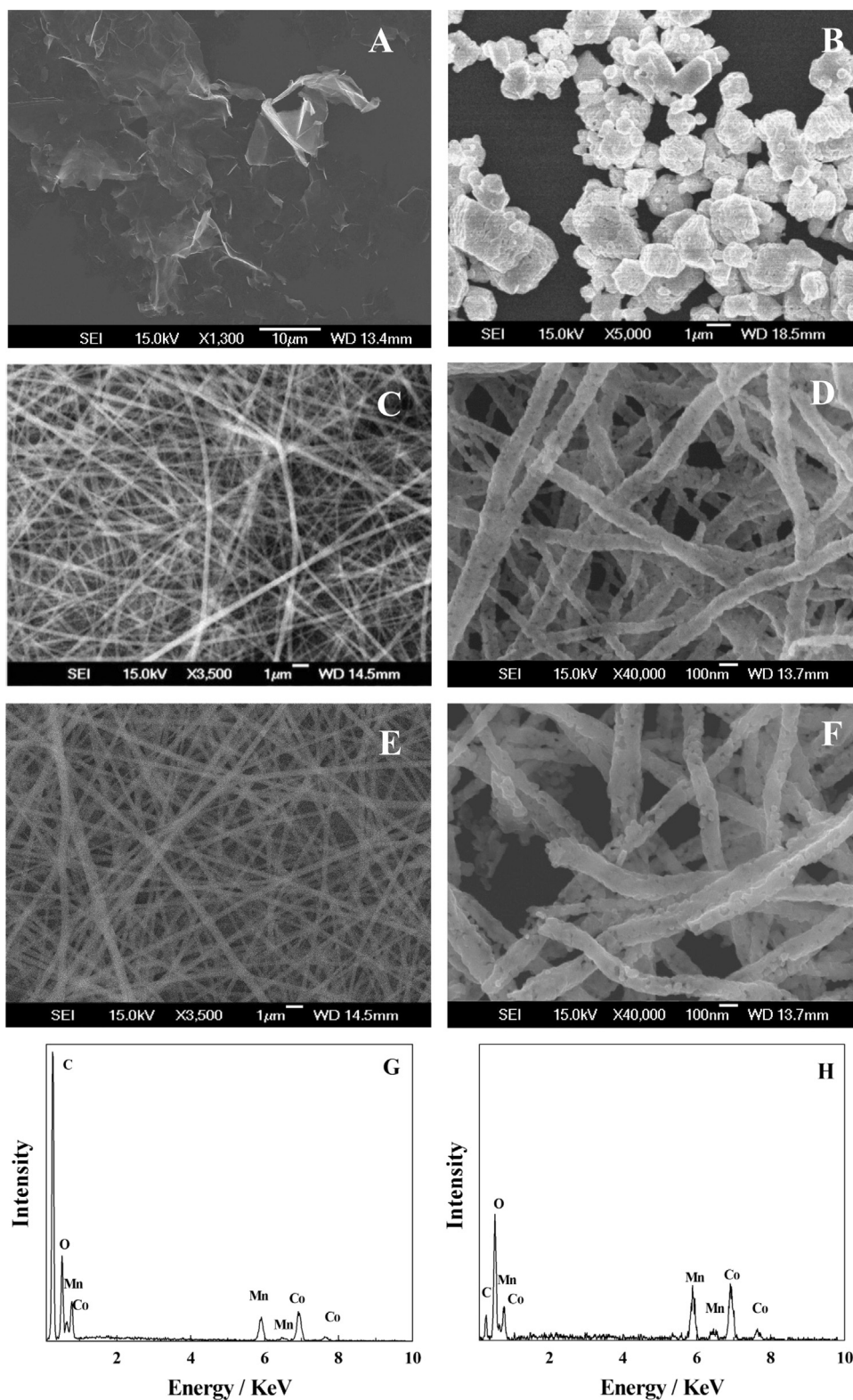
Fig. 2. SEM images of the as-prepared graphene (A), MCNPs (B), electrospun GMCFs before (C) and after calcination (D), electrospun MCFs before (E) and after calcination (F); EDS of electrospun GMCFs (G) and MCFs (H).

EDS measurements were performed to investigate the chemical composition of the synthesized GMCFs. Fig. 2G and H shows EDS of the prepared GMCFs and MCFs. According to EDS analysis, C, Mn, Co and O were the major constituents of the samples. Quantitative EDS analysis indicated a 1:2 atomic ratio of Mn: Co, which was the typical chemical composition of manganese cobalt spinel.

This is in accordance with the X-ray powder diffraction result. In addition, the C peak of GMCFs had higher intensity than that of MCFs, which may be attributed to the presence of graphene.

The detailed morphology and crystalline structure of the nanofibers were further investigated by TEM. As shown in Fig. 3A, GMCFs were composed of numerous nanoparticles which were
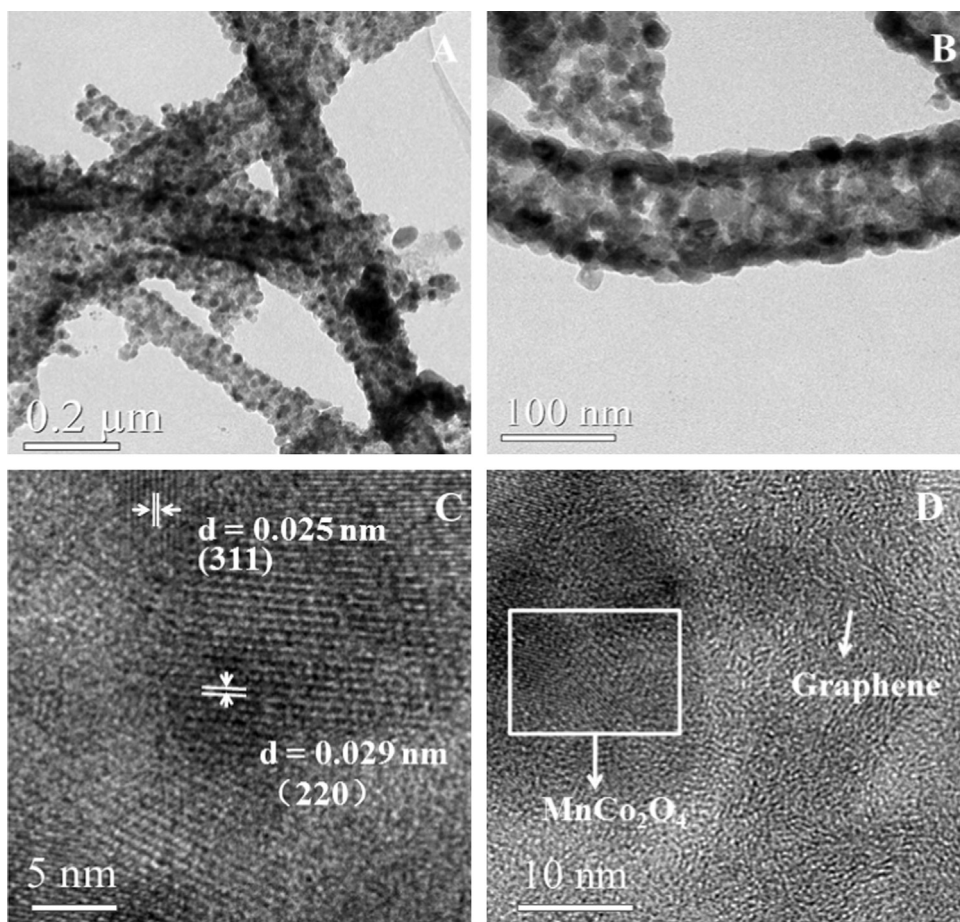
Fig. 3. TEM image of electrospun GMCFs (A), high magnification TEM image of electrospun GMCFs (B); HRTEM images of electrospun MCFs (C) and GMCFs (D).

loosely connected with each other and stacked along the nanofibers. The high magnification TEM image revealed the shape and size of the nanoparticles in nanofibers. In Fig. 3B, the irregular spherical $MnCo_2O_4$ nanoparticles became obvious and formed nanofibers with an average size of 20 nm. Crystalline lattice structures of MCFs and GMCFs are clearly shown in the high-resolution TEM (HR-TEM) images. HR-TEM image (Fig. 3C) illustrated that the lattice fringes of MCFs exhibited interplanar spacing of 0.025 and 0.029 nm, which were indexed to the crystal faces (311) and (220) of spinel phase, respectively. Lattice fringes of graphene can be discerned in Fig. 3D with d-spacing of 0.38 nm corresponding to the (002) crystallographic plane. These results indicate that the presence of graphene phase has little influence on the crystallinity of spinel.

To further confirm the presence and dispersion state of atoms in GMCFs, HRTEM mapping was performed on selected area of a nanofiber in high magnification. The corresponding elemental mapping of graphene decorated $MnCo_2O_4$ nanofiber provided information on the distribution of Mn, Co and C atoms in the nanofiber (see Supporting information, Fig. S1).

3.3. Electrochemical characterization

In order to test the electrochemical properties of different electrodes, cyclic voltammetry (CV) and electrochemical impedance spectroscopy (EIS) were obtained at different electrodes in 5 mM $[Fe(CN)_6]^{3-/4-}$ (1:1)+0.1M KCl solution. In Fig. 4A, compared to those at the bare electrode, the peak current (I_p) of $[Fe(CN)_6]^{3-/4-}$ at MCF/GCE (curve b) was lower and potential difference between the oxidation and reduction peaks (ΔE_p)

became larger (curve a), suggesting that redox reversibility of $[Fe(CN)_6]^{3-/4-}$ became poorer, which was caused by the semiconductor property of spinel. After the electrode was modified with GMCFs (curve c), I_p increased and ΔE_p decreased compared with those at the MCF/GCE, indicating that graphene played a role in increasing the electroconductivity of MCFs.

EIS was also employed to monitor interfacial properties of the electrode surface. Generally speaking, the semicircular part of Nyquist plot at higher frequencies corresponds to the electron-transfer-limited process and the diameter is equivalent to the electron transfer resistance (R_{et}) (Zhu et al., 2010). Fig. 4B illustrates the Nyquist diagrams of bare GCE (a), MCF/GCE (b) and GMCF/GCE (c) in 5 mM $[Fe(CN)_6]^{3-/4-}$ (1:1)+0.1M KCl solution. Compared to that of the bare electrode, R_{et} of MCF/GCE increased from 230 Ω (curve a) to 1050 Ω (curve b); While compared to that of MCF/GCE, R_{et} of GMCF/GCE (curve c) decreased to 650 Ω. The results confirm that the incorporation of graphene into MCFs can decrease the electron transfer resistance of catalytic materials.

The cyclic voltammetric behaviors of GCE (a), MCF/GCE (b) and GMCF/GCE (c) were investigated in 0.2 M NaOH solution in the absence (curves a, b and c) and presence (curves a′, b′ and c′) of 1.0 mM glucose. As shown in Fig. 4C, two pairs of redox peaks at +0.08/+0.10 V and +0.45/+0.50 V were observed on GMCF/GCE (curve c), corresponding to redox peaks of Co and Mn, respectively (B. Ding et al., 2010; Y. Ding et al., 2010; Mho and Johnson, 2001). When 1.0 mM glucose was added into 0.2 M NaOH, the peak current of glucose on GMCF/GCE (curve c′) remarkably increased, while no obvious electrochemical response was observed at GCE (curve a′). The average current of 10 μM glucose obtained on GMCF/GCE was 1.83 μA (Fig. 4C, inset), which was much larger
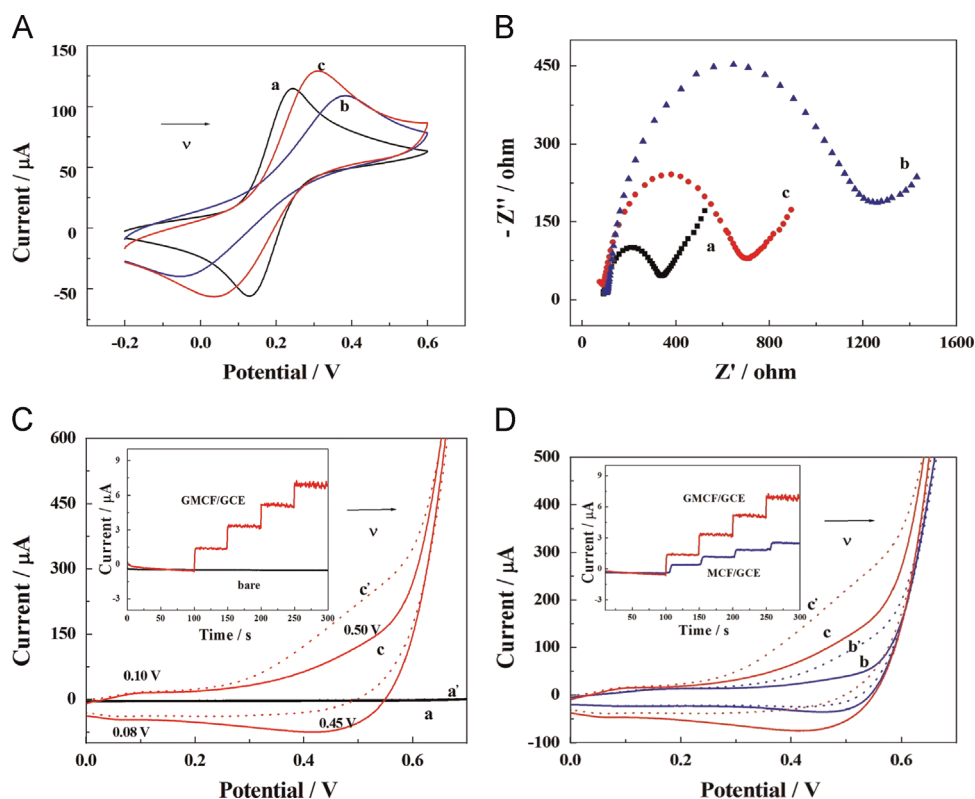
Fig. 4. CVs (A) and EIS (B) recorded in 5.0 mM [Fe(CN)$_6$]$^{3-/4-}$ +0.1 M KCl at the GCE (a), MCF/GCE (b) and GMCF/GCE (c); CVs of the bare GCE, MCF/GCE and GMCF/GCE in the absence (curves a, b and c) and presence (curves a′, b′ and c′) of 1 mM glucose in 0.2 M NaOH at a scan rate of 100 mV s^{-1}. Inset: current–time curves obtained on GCE, MCF/GCE and GMCF/GCE upon successive additions of 10 μM glucose.

than that obtained on bare GCE, illustrating GMCF/GCE showed excellent electrocatalytic activity towards glucose. In Fig. 4D, the redox peaks of Co and Mn were observed on MCF/GCE and GMCF/GCE, while the peak currents on GMCF/GCE (curve c) were higher than that of MCF/GCE (curve b) and the peak potentials shifted negatively, which may be attributed to the synergistic effect of MCFs and graphene. The average current obtained on GMCF/GCE was 2.41 times as much as that obtained on MCF/GCE (Fig. 4D, inset), which can further indicate the admirable electrocatalytic activity of electrospun GMCFs.

The above electrochemical studies reveal the electrocatalytic activity of GMCFs modified GCE towards non-enzymatic glucose oxidation. The spinel-type MnCo$_2$O$_4$ nanoparticles in nanofibers may play an important role for the oxidation of glucose. The possible reaction mechanism can be illustrated in Scheme S1 (see Supporting information). When applying a potential of +0.55 V to the modified electrode, GMCFs–Mn(II)Co(II) loses two electrons and is oxidized to strong oxidizing agent GMCFs(OH)$_2$–Mn(III)Co(III), which can oxidize glucose to gluconolactone. At the same time, the graphene in nanofibers will accelerate the rate of electron transfer and promote the catalytic activity of redox couples (Z. Zhang et al., 2012; Hou et al., 2012).

3.4. Amperometric detection of glucose

Experimental parameters possibly influencing the analytical performance of the non-enzymatic sensor were optimized, including supporting electrolyte (NaOH), applied potential and the concentration of modifier. The results show that the optimized experimental conditions are 0.2 M NaOH, +0.55 V, and

4.0 mg mL^{-1} GMCFs, respectively (see Supporting information, Fig. S2).

Under optimal conditions, amperometric responses upon successive addition of glucose were detected on GMCF/GCE in 0.20 M NaOH at +0.55 V. The typical amperometric response curves of different concentrations of glucose are shown in Fig. 5. A well-defined, stable and fast amperometric response increasing stepwise with the level of glucose within 1.5 s can be observed, demonstrating efficient catalytic ability of GMCF/GCE for glucose electro-oxidation. The current responses are linear with glucose concentrations from 0.005 to 800 μM (Fig. 5B), with the regression equation as: I_p (μA)=1.543+0.114 C (M) (R=0.995). The detection limit is estimated to be 0.001 μM (S/N=3) and the sensitivity is 1813.8 μA mM^{-1} cm^{-2}. For comparison, the performances of GMCF/GCE and other glucose sensors reported in literature have been listed in Table S1 (see Supporting information), showing that GMCF/GCE exhibits prominent electrocatalytic performance for glucose sensing in terms of the linear range, detection limit and sensitivity (Ma and Nakazato, 2014; J.Y. Wang et al., 2013; Y.Z. Wang et al., 2013; Umar et al., 2009; Palanisamy et al., 2012; Zhang et al., 2010; Z. Zhang et al., 2012; Y.Q. Zhang et al., 2012).

The batch-to-batch reproducibility at three individually modified electrodes gave the relative standard deviation (RSD) of 4.16% for amperometric response to glucose. Nine successive measurements of glucose on the same GMCF/GCE yielded a RSD of 1.72%. The stability of the non-enzymatic sensor was evaluated through the amperometric responses of 10 μM glucose recorded over a month. The electrode was stored at room temperature and tested every 5 days (see Supporting information, Fig. S3A). The current response of GMCF/GCE was approximately 90% of its original counterpart.
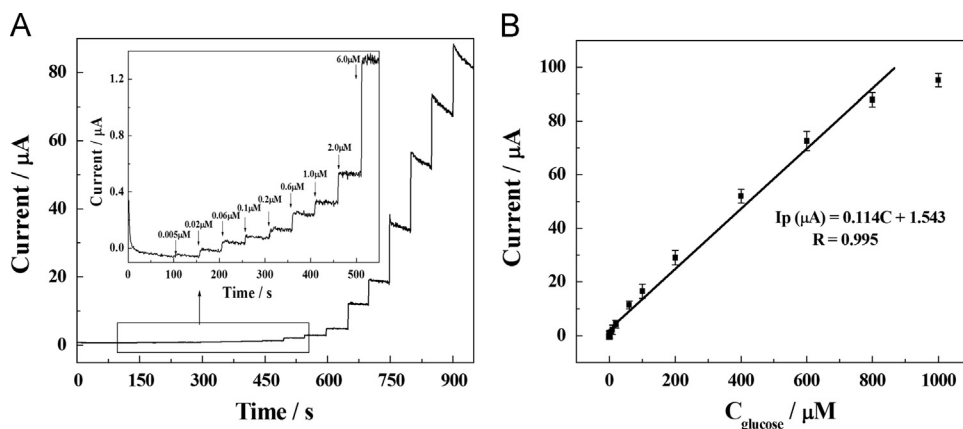
Fig. 5. (A) Current–time curves obtained at GMCF/GCE upon different concentrations of glucose in 0.2 M NaOH at +0.55 V. Inset: current–time responses for low concentrations; (B) relationship between the amperometric responses and the glucose concentrations.

Anti-interference property is crucial for a non-enzymatic electrochemical biosensor. The interference from other compounds normally coexisting with glucose in real samples such as uric acid (UA), dopamine (DA), ascorbic acid (AA), tryptophan (Trp), glycine (Gly), galactose (Gal), sucrose (Suc) and maltose (Mal), may cause accuracy problems in glucose determination. The glucose level is at least 30 times higher than those of interfering species in human blood, therefore the interference experiment was carried out by adding 150 μM glucose with 5 μM of each interfering substances (see Supporting information, Fig. S3B). As a result, compared to glucose, these species produce negligible current responses, revealing that GMCF/GCE can be used for the specific detection of glucose in blood samples under physiological conditions.

To verify the reliability of the sensor for routine analysis, the sensor was applied for the determination of glucose in real blood serum samples. Before electrochemical detection, the serum was handled by perchloric acid to remove protein, then 10 μL disposed serum sample was diluted in a 10 mL 0.2 M NaOH solution. The quantitative determination of glucose was analyzed by the standard addition method. In order to confirm the accuracy of this method, HEA-214 glucometer (a commercial blood glucose meter manufactured by Omron Co. Ltd., China) was used to measure glucose in serum samples in comparison with GMCFs modified electrode. The results reveal that the fabricated non-enzyme sensor can be utilized for practical sample testing with favorable accuracy and precision (see Supporting information, Table S2).

4. Conclusions

This work developed a simple and fast method to synthesize GMCFs by electrospinning technique and subsequent calcination in an Ar atmosphere. The outstanding electron-transfer ability of the electrocatalyst GMCFs was improved by two effective approaches: electrospinning can prevent magnetic particles from aggregating by processing the materials into nanofibers with large surface area; graphene embedded into MCFs can greatly improve the conductivity of the nanofibers. The novel GMCFs can be used as the electrocatalysts for quantitative determination of glucose with high sensitivity and selectivity, which hold unique promising future for application in non-enzymatic glucose biosensors.

Appendix A. Supporting information

Supplementary data associated with this article can be found in the online version at http://dx.doi.org/10.1016/j.bios.2014.11.040.

References

Borodko, Y., Habas, S.E., Koebel, M., Yang, P.D., Frei, H., Somorjai, G.A., 2006. J. Phys. Chem. B 110, 23052–23059.
Cheng, F.Y., Shen, J., Peng, B., Pan, Y.D., Tao, Z.L., Chen, J., 2011. Nat. Chem. 3 (281), 79–84.
Cheng, Y.L., Zou, B.L., Yang, J.L., Wang, C.J., Liu, Y.J., Fan, X.Z., Zhu, L., Wang, Y., Ma, H. M., Cao, X.Q., 2011. CrystEngComm 13, 2268–2272.
Chen, J.H., Shi, W.B., Zhang, X.Y., Arandiyan, H., Li, D.F., Li, J.H., 2011. Environ. Sci. Technol. 45, 8491–8497.
Ding, B., Wang, M., Wang, X., Yu, J., Sun, G., 2010. Mater. Today 13, 16–27.
Ding, Y., Wang, Y., Su, L., Bellagamba, M., Zhang, H., Lei, Y., 2010. Biosens. Bioelectron. 26, 542–548.
Dong, Q., Wang, G., Hu, H., Yang, J., Qian, B.Q., Ling, Z., Qiu, J.S., 2013. J. Power Sources 243, 350–353.
Ferrari, A.C., Meyer, J.C., Scardaci, V., Casiraghi, C., Lazzeri, M., Mauri, F., Piscanec, S., Jiang, D., Novoselov, K.S., Roth, S., Geim, A.K., 2006. Phys. Rev. Lett. 97, 187401–187405.
Geim, A.K., Novoselov, K.S., 2007. Nat. Mater. 6, 183–191.
Hummers, W.S., Offeman, R.E., 1958. J. Am. Chem. Soc. 80, 1339.
Hu, L.F., Wu, L.M., Liao, M.Y., Hu, X.H., Fang, X.S., 2012. Adv. Funct. Mater. 22, 998–1004.
Huang, R., Ikuhara, Y.H., Mizoguchi, T., Findlay, S.D., Kuwabara, A., Fisher, C.A.J., Moriwake, H., Oki, H., Hirayama, T., Ikuhara, Y., 2011. Angew. Chem. Int. Ed. 50, 3053–3057.
Heller, A., Feldman, B., 2008. Chem. Rev. 108, 2482–2505.
Hou, L.R., Yuan, C.Z., Yang, L., Shen, L.F., Zhang, F., Zhang, X.G., 2011. RSC Adv. 1, 1521–1526.
Hou, C.T., Xu, Q., Yin, L.N., Hu, X.Y., 2012. Analyst 137, 5803–5808.
Imran, M., Kim, D.H., Al-Masry, W.A., Mahmood, A., Hassan, A., Haider, S., Ramay, S. M., 2013. Polym. Degrad. Stab. 98, 904–915.
Jo, M.R., Jung, Y.S., Kang, Y.M., 2012. Nanoscale 4, 6870–6875.
Kovtyukhova, N.I., Ollivier, P.J., Martin, B.R., Mallouk, T.E., Chizhik, S.A., Buzaneva, E. V., Gorchinskiy, A.D., 1999. Chem. Mater. 11, 771–778.
Liu, M., Yin, X.B., Ulin-Avila, E., Geng, B.S., Zentgraf, T., Ju, L., Wang, F., Zhang, X., 2011. Nature 474, 64–67.
Lv, W., Tang, D.M., He, Y.B., You, C.H., Shi, Z.Q., Chen, X.C., Chen, C.M., Hou, P.X., Liu, C., Yang, Q.H., 2009. ACS Nano 3, 3730–3736.
Li, D., Xia, Y.N., 2004. Adv. Mater. 16, 1151–1170.
Li, F., Liu, J.J., Evans, D.G., Duan, X., 2004. Chem. Mater. 16, 1597–1602.
Li, J., Lin, X., 2007. Biosens. Bioelectron. 22, 2898–2905.
Lin, D.D., Wu, H., Zhang, R., Pan, W., 2009. Chem. Mater. 21, 3479–3484.
Liang, Y.Y., Wang, H.L., Zhou, J.G., Li, Y.G., Wang, J., Regier, T., Dai, H.J., 2012. J. Am. Chem. Soc. 134, 3517–3523.
Lucchese, M.M., Stavale, F., Martins Ferreira, E.H., Vilani, C., Moutinho, M.V.O., Capaz, R.B., Achete, C.A., Jorio, A., 2010. Carbon 48, 1592–1597.
Ma, Q., Nakazato, K., 2014. Biosens. Bioelectron. 51, 362–365.
Meyer, J.C., Geim, A.K., Katsnelson, M.I., Novoselov, K.S., Booth, T.J., Roth, S., 2007. Nature 446, 60–63.
Mho, S., Johnson, D.C., 2001. J. Electroanal. Chem. 495, 152–159.
Nan, D., Wang, J.G., Huang, Z.H., Wang, L., Shen, W., Kang, F., 2013. Electrochem. Commun. 34, 52–55.
Newman, J.D., Turner, A.P.F., 2005. Biosens. Bioelectron. 20, 2435–2453.

Niyogi, S., Bekyarova, E., Itkis, M.E., McWilliams, J.L., Hamon, M.A., Haddon, R.C., 2006. J. Am. Chem. Soc. 128, 7720–7721.

Novoselov, K.S., Geim, A.K., Morozov, S.V., Jiang, D., Zhang, Y., Dubonos, S.V., Grigorieva, I.V., Firsov, A.A., 2004. Science 306, 666–669.

Ouyang, Z.F., Li, J.F., Wang, J.H., Li, Q., Ni, T.Y., Zhang, X.Y., Wang, H.X., Li, Q., Su, Z.Q., Wei, G., 2013. J. Mater. Chem. B 1, 2415–2424.

Palanisamy, S., Chen, S.M., Sarawathi, R., 2012. Sens. Actuators B 166–167, 372–377.

Paudel, T.R., Zakutayev, A., Lany, S., d'Avezac, M., Zunger, A., 2011. Adv. Funct. Mater. 21, 4493–4501.

Rojas, R.M., Vila, E., Garcia, O., de Vidales, J.L.M., 1994. J. Mater. Chem. 4, 1635–1639.

Rousseau, D.L., Bauman, R.P., Porto, S.P.S., 1981. J. Raman Spectrosc. 10, 253–290.

Saquing, C.D., Manasco, J.L., Khan, S.A., 2009. Small 5, 944–951.

Shan, C., Yang, H., Song, J., Han, D., Ivaska, A., Niu, L., 2009. Anal. Chem. 81, 2378–2382.

Stoller, M.D., Park, S., Zhu, Y., An, J., Ruoff, R.S., 2008. Nano Lett. 8, 3498–3502.

Tang, C., Saquing, C.D., Harding, J.R., Khan, S.A., 2010. Macromolecules 43, 630–637.

Umar, A., Rahman, M.M., Al-Hajry, A., Hahn, Y.B., 2009. Electrochem. Commun. 11, 278–281.

Wang, D., Li, X., Wang, J., Yang, J., Geng, D., Li, R., Cai, M., Sham, T.K., Sun, X., 2012. J. Phys. Chem. C 116, 22149–22156.

Wang, J.P., Thomas, D.F., Chen, A.C., 2008. Anal. Chem. 80, 997–1004.

Wang, J.Y., Chen, L.C., Ho, K.C., 2013. ACS Appl. Mater. Interfaces 5, 7852–7861.

Wang, Y.Z., Zhong, H., Li, X.M., Jia, F.F., Shi, Y.X., Zhang, W.G., Cheng, Z.P., Zhang, L.L., Wang, J.K., 2013. Biosens. Bioelectron. 48, 56–60.

Wang, S.G., Zhang, Q., Wang, R.L., Yoon, S.F., Ahn, J., Yang, D.J., Tian, J.Z., Li, J.Q., Zhou, Q., 2003. Electrochem. Commun. 5, 800–803.

Wilson, R., Turner, A.P.F., 1992. Biosens. Bioelectron. 7, 165–185.

Wu, H.X., Cao, W.M., Li, Y., Liu, G., Wen, Y., Yang, H.F., Yang, S.P., 2010. Electrochim. Acta 55, 3734–3740.

Wu, J.W., Wang, C.H., Wang, Y.C., Chang, J.K., 2013. Biosens. Bioelectron. 46, 30–36.

Yang, X.W., Cheng, C., Wang, Y.F., Qiu, L., Li, D., 2013. Science 534, 534–537.

Yoshimatsu, K., Ye, L., Lindberg, J., Chronakis, I.S., 2008. Biosens. Bioelectron. 23, 1208–1215.

Zeng, Z., Natesan, K., Cai, Z., Darling, S.B., 2008. Nat. Mater. 7, 641–646.

Zhang, H.M., Yu, X.Z., Guo, D., Qu, B.H., Zhang, M., Li, Q.H., Wang, T.H., 2013. ACS Appl. Mater. Interfaces 5, 7335–7340.

Zhang, L., Ni, Y.H., Li, H., 2010. Microchim. Acta 171, 103–108.

Zhang, Y.T., Luo, L.Q., Zhang, Z., Ding, Y.P., Liu, S., Deng, D.M., Zhao, H.B., Chen, Y.G., 2014. J. Mater. Chem. B 2, 529–535.

Zhang, Z., Gu, S.Q., Ding, Y.P., Jin, J.D., 2012. Anal. Chim. Acta 745, 112–117.

Zhang, Y.Q., Wang, Y.Z., Jia, J.B., Wang, J.G., 2012. Sens. Actuators B 171–172, 580–587.

Zhu, L.M., Luo, L.Q., Wang, Z.X., 2012. Biosens. Bioelectron. 35, 507–511.

Zhu, J.K., Gao, Q.M., 2009. Microporous Mesoporous Mater. 124, 144–152.

Zhu, Z.H., Li, X., Zeng, Y., Sun, W., 2010. Biosens. Bioelectron. 25, 2313–2317.

Zou, Y.J., Xiang, C.L., Sun, L.X., Xu, F., 2008. Biosens. Bioelectron. 23, 1010–1016.